Chromosome organization by a nucleoid-associated protein in live bacteria

Wenqin Wang[1,†], **Gene-Wei Li**[1,2,†], **Chongyi Chen**[2,3,†], **X. Sunney Xie**[2,*], and **Xiaowei Zhuang**[1,2,4,*]

[1]Department of Physics, Harvard University, Cambridge, MA 02138.

[2]Department of Chemistry and Chemical Biology, Harvard University, Cambridge, MA 02138.

[3]Department of Molecular and Cellular Biology, Harvard University, Cambridge, MA 02138.

[4]Howard Hughes Medical Institute, Harvard University, Cambridge, MA 02138.

Abstract

Bacterial chromosomes are confined in submicron-sized nucleoids. Chromosome organization is facilitated by nucleoid-associated proteins (NAPs), but the mechanisms of action remain elusive. Here we used super-resolution fluorescence microscopy, in combination with a chromosome-conformation capture assay, to study the distributions of major NAPs in live *E. coli* cells. Four NAPs, HU, Fis, IHF, and StpA, were largely scattered throughout the nucleoid. In contrast, H-NS, a global transcriptional silencer, formed two compact clusters per chromosome driven by oligomerization of DNA-bound H-NS through interactions mediated by the amino-terminal domain of the protein. H-NS sequestered the regulated operons into these clusters and juxtaposed numerous DNA segments broadly distributed throughout the chromosome. Deleting H-NS led to substantial chromosome reorganization. These observations demonstrate that H-NS plays a key role in global chromosome organization in bacteria.

The structure of the bacterial chromosome and the molecular mechanisms underlying its organization are poorly understood, in part due to the lack of appropriate tools for visualizing the chromosome in vivo. It has been shown by fluorescence microscopy that DNA only occupies the central part of the bacterial cell, referred to as the nucleoid (*1*), but the diffraction-limited optical resolution prevents a detailed characterization. Ultrastructural characterization of the nucleoid by electron microscopy has provided varying results depending on the procedures used to fix, dehydrate, and embed the cells (*1-2*). Recently, labeling of specific gene loci using fluorescence in situ hybridization and fluorescent repressor-operator systems has allowed imaging of individual gene positions, and their relationship to DNA replication and segregation, in fixed and live bacterial cells (*3-5*). However, these studies probe only a set of specific loci at a time, and the global chromosome organization remains unclear.

In bacteria, major nucleoid-associated proteins (NAPs) are the most abundant factors that associate with the chromosome (*6-7*). In *E. coli*, major NAPs include H-NS, HU, Fis, IHF, and StpA (*6*). Each of these NAPs binds up to hundreds of specific sites per chromosome (*6, 8-9*). Moreover, due to their substantial nonspecific DNA-binding affinity, the majority of cellular NAPs are bound to the chromosomal DNA with a coverage of about one NAP per 100 base pairs of DNA (*10*). NAPs have two major functions: gene regulation and

---

[*]To whom correspondence should be addressed. xie@chemistry.harvard.edu, zhuang@chemistry.harvard.edu.
[†]These authors contributed equally to the work.

chromosome organization (*7*). In particular, H-NS preferentially binds to AT-rich sequences (*8-9, 11-13*), functions as a global transcriptional silencer of genes with high AT content (*14-15*), and is thought to reside at the center of the nucleoid (*16*). The oligomerization of H-NS can promote higher-order DNA structures in vitro (*17*), potentially through DNA looping, bridging, and/or stiffening (*18-20*). It has been hypothesized based on these biophysical properties of NAPs and their numerous binding sites on DNA that NAPs potentially act as chromosome organizing centers (*21*). However, it remains unknown whether the implicated higher-order DNA structures induced by NAPs exist in vivo, and how the chromosome is globally organized by the NAPs.

In a live bacterial cell, a single protein, upon binding to the less mobile structures, such as the cell membrane or chromosome, can be detected and localized against a strong cellular autofluorescence background (*22-24*). However, the diffraction-limited optical resolution limits this imaging approach to proteins with low copy numbers in the cell (*24*). To obtain the subcellular distribution and organization of the abundant bacterial NAPs, sub-diffraction-limit image resolution is required.

Here, we used localization-based super-resolution imaging (stochastic optical reconstruction microscopy (STORM) or photoactivated localization microscopy) (*25-29*) to survey the subcellular distributions of major NAPs, H-NS, HU, Fis, IHF, and StpA. We tagged the target of interest with a monomeric photoactivatable fluorescent protein, mEos2 (*30*), unless otherwise specified. We then created *E. coli* strains in which the fusion proteins were expressed from their native promoters at the endogenous loci, allowing the targets to be fully labeled and expressed approximately at the wildtype level (Table S1) (*31*). All of these mEos2 fusion strains exhibited the same growth rates (cell doubling times) as the wildtype (*31*). Cells were imaged in a M9 minimal medium supplemented with glucose at room temperature shortly after taken out of the 37°C culture at the early log phase (*31*).

To acquire a super-resolution image, the mEos2 molecules were activated by a weak 405 nm light, such that only an optically resolvable subset of molecules were activated at any given instant; the activated molecules were imaged using a 561 nm light and their centroid positions were determined in three dimensions (3D) using astigmatism imaging, as previously shown in 3D STORM (*32*). The molecular localizations accumulated over time allowed a sub-diffraction-limit image to be constructed. A continuous activation and imaging mode (*33*) was used, allowing ~1,000 molecules per cell to be imaged every minute. We note that only a subset of the mEos2 label could mature and become fluorescent due to the long maturation time of mEos2 compared to the *E. coli* doubling time (*30*). Among those that matured, only a subset could be activated by the 405 nm light. The laser illumination used for imaging did not exert appreciable effect on cell viability, as evident from the nearly identical (within 10%) cell doubling times observed with or without illuminations.

Notably, H-NS formed a few compact clusters within each cell (Fig. 1A, Movie S1). The majority of H-NS molecules resided in these clusters, whose fluorescence accounted for 60 ± 25% of the total activated mEos2 signal (*31*). To test the functional integrity of the mEos2-tagged H-NS, we measured the expression levels of *hdeA* and *hchA*, two genes repressed by H-NS (*15*). Indeed, the strain expressing the fluorescent fusion protein retained wildtype activity in repressing these two genes (Fig. S1) (*31*). As a control, the expression levels of *lacZ*, a gene not regulated by H-NS, were similar in the wildtype, fluorescent fusion, as well as H-NS deletion strains (Fig. S1).

In contrast to the clustered distribution of H-NS, HU was largely scattered throughout in the nucleoid (Fig. 1B), consistent with recent data from another bacterial species, *C. crescentus*

(*34*). Similar distributions were observed for Fis and IHF, albeit at lower expression levels (Fig. S2) (*31*). StpA also displayed a scattered distribution in the nucleoid (Fig. S2), despite being a paralogue of H-NS (*14*). Interestingly, Rok, a *B. subtilis* protein functionally analogous to H-NS but lacking any sequence homology, is distributed non-uniformly in the nucleoid (*35*). In addition to the NAPs, we also imaged the ribosomes, which should be excluded from the nucleoid (*1*). As expected, the ribosomes were enriched in the cell periphery (Fig. S3) (*31*).

Next, we examined the molecular mechanisms responsible for the formation of H-NS clusters in vivo. H-NS has two structural domains: an N-terminal domain that promotes dimerization and oligomerization and a C-terminal domain that binds to DNA (*17-19*). We tested the effects of these functions on the cluster formation by introducing an N-terminal point mutation L30P that inhibits H-NS dimerization (*36*) or a C-terminal point mutation P116S that inhibits DNA binding (*37-38*) into the chromosomally expressed H-NS-mEos2 fusion protein. The expression levels of the two mutants were comparable to that of the wildtype (Table S1) (*31*). Both mutations abolished the silencing effect of H-NS on *hdeA* and *hchA*, but had little influence on *lacZ* expression (Fig. S1). In contrast to the wildtype H-NS, H-NS^{L30P} did not form clusters, but was scattered throughout the nucleoid (Fig. 1C), indicating that cluster formation was induced by the N-terminal-domain driven oligomerization of the protein. In the cells expressing H-NS^{P116S}, the number of observed localizations was reduced by ~20 fold compared to the H-NS expressing cells (Fig. 1D), indicating that the localizations of H-NS were primarily due to molecules bound to DNA.

To quantify the effect of H-NS clustering on chromosome organization, we first characterized the number of H-NS clusters per chromosome, and the physical location and size of these clusters. Given the cylindrical symmetry of the cells and that the H-NS clusters were rarely observed to line up with each other in the *z*-direction, we used 2D projection images for the following quantitative characterizations to take advantage of the superior resolution in the *xy* plane (measured to be ~35 nm in full width at half maximum (FWHM)) compared to that along the *z* direction (~75 nm, FWHM) (*31*).

Most newly divided cells had approximately two clusters, and the number increased with the cell length (Fig. 2A, B). For the longest cells prior to division, the cluster number reached four on average (Fig. 2B). These data suggest an increase in the number of H-NS clusters with the chromosome copy number. To test whether the specific fluorescent protein tag, mEos2, had influenced the cluster formation, we fused H-NS with a different monomeric photoactivatable fluorescent protein, PAmCherry1 (*39*). Similar clustering was observed for PAmCherry1-labeled H-NS (Fig. S4). Subsequent analyses of H-NS clusters were performed on mEos2-labeled samples.

To determine the number of clusters per chromosome, we reduced the cell growth rate by using a glycerol-supplemented minimal medium to ensure that each newly divided cell had exactly one copy of the chromosome (*31*). Under this condition, we observed two H-NS clusters in the shortest cells (Fig. 2C), suggesting that there are ~2 H-NS clusters associated with each copy of the chromosome. These two clusters were preferentially located near the one-quarter and three-quarter positions along the long axis of the cell (Fig. 2D). In cells that had three clusters, the additional cluster tended to appear in the middle (Fig. S5) (*31*).

To characterize the cluster size, we determined the localization distributions within the clusters. The widths of the distributions were on average ~160 nm measured at half maximum density and ~360 nm at 3% of the maximum (Fig. 2E). The background localization density outside the clusters was only ~1% of the peak densities in the clusters. The cluster size was substantially larger than both our localization precision (~35 nm) and

the cluster movement during the observation time (~40 - 50 nm over 0.5 - 2 min). Moreover, the measured cluster size did not change appreciably when we changed the imaging time from 0.5 to 1 min. These results indicate that neither localization precision nor motion blurring had substantial effects on our measurements on the H-NS clusters.

The above quantifications indicate that the volume occupied by the H-NS clusters in each cell represents only a small fraction of the total nucleoid volume that was estimated to be ~0.2 μm^3 from the volume occupied by HU molecules as well as from previous experiments (*40*). Given that H-NS binding sites are broadly distributed throughout the *E. coli* genome (*8-9*), collapsing of the DNA-bound H-NS into two compact clusters must therefore lead to substantial folding of DNA and reorganization of the chromosome at the global scale.

To probe whether the cluster organization of H-NS correlates with its regulatory role, we studied the spatial relationship between H-NS clusters and H-NS regulated genes. The positions of the gene loci were determined by imaging eYFP-labeled Tet repressor (TetR-eYFP) bound to *tet* operator (*tetO*) sequences inserted upstream of the genes of interest (Fig. 3A). Unlike previously used fluorescent repressor-operator systems, which typically contain tens to hundreds of tandem repeats of repressor binding sites, we inserted only six *tetO* repeats (219 bp) immediately upstream of the target genes to more precisely mark their positions. Using a negative feedback loop regulated by MalI (Fig. 3A) (*41*), we achieved a low expression level of TetR-eYFP that allowed the clear detection of the *tetO*-bound TetR-eYFP above the background (Fig. 3B), though not all target loci were necessarily bound by TetR-eYFP due to the small number of *tetO* sites and the low expression level of TetR-eYFP. These strains had the same growth rates as the wildtype (*31*), whereas the strains with a large number of inserted repressor binding sites tend to exhibit growth defects.

The two-color super-resolution images of mEos2-labeled H-NS and eYFP-labeled gene loci were taken using a sequential imaging approach to avoid the spectral crosstalk between eYFP and the pre-activation form of mEos2: The mEos2 molecules were first activated using a 405 nm laser and imaged with a 561 nm laser; after all mEos2 molecules were photobleached, the eYFP molecules were imaged using a 514 nm laser. The negligible displacement of the H-NS clusters (~20 nm) during the time taken for eYFP imaging allowed the colocalization between the gene loci and H-NS clusters to be probed in live cells.

Using this approach, we imaged H-NS together with the loci of *hdeA, hchA*, and *lacZ* genes, the former two of which are regulated by H-NS (Fig. S1). As shown in Fig. 3B, C, *hdeA* and *hchA* colocalized with H-NS clusters to a substantially larger extent than *lacZ*, indicating that the H-NS-regulated operons are preferentially sequestered into the H-NS clusters. Interestingly, while the H-NS clusters themselves appeared largely static, both *hdeA* and *hchA* loci were mobile and did not always colocalize with the clusters, suggesting that the nucleoprotein complex is a heterogeneous and dynamic entity.

By sequestering the regulated genes, the H-NS clusters likely cause a significant reorganization of the chromosome. To test this effect, we probed the positions of *hdeA, hchA* and *lacZ* in the wildtype versus *hns*-null strains. The position of the labeled gene locus was determined relative to the cell's long and short axes, and Fig. 3D shows the probability density maps of these gene loci obtained from many cells. Notably, the positions of *hdeA* and *hchA* loci in *hns*-null cells were both shifted by ~300 nm compared to the wildtype cells, a distance comparable to the radius of the nucleoid. In contrast, the position of the *lacZ* gene remained largely unchanged (shifted by less than 60 nm) upon *hns* deletion.

To further test the long-range chromosome interactions induced by H-NS clustering, we performed a chromosome conformation capture (3C) assay (*42*) to probe the spatial

proximity among various H-NS regulated genes. In this assay, DNA segments brought into proximity by protein-mediated interactions were captured by formaldehyde crosslinking, followed by restriction enzyme digestion. The crosslinked DNA segments were then ligated and probed by quantitative PCR (qPCR) with specifically designed primer pairs. The amount of PCR products relative to those obtained from non-crosslinked cells should scale with the crosslinking frequency, which in turn reflects the relative proximity between the DNA segments.

Using this approach, we tested the pair-wise proximity among nine H-NS regulated genes broadly distributed along the *E. coli* genome (Fig. 4A), which gave a total of 36 possible pairs. In addition, we selected three random loci on the genome plus *lacZ* as four negative control sites (Fig. 4A). The six pairs among these four sites and the nine pairs between *lacZ* and each of the nine H-NS regulated genes constituted a total of 15 control pairs. Out of the 36 pairs of H-NS-regulated gene loci, ten showed PCR priming errors, while the remaining 26 pairs gave quantifiable results. Likewise, 14 out of 15 control pairs gave quantifiable results. Because all control pairs showed crosslinking frequencies < 2 (Fig. 4B, right), we designated 2 as the background value. The vast majority of the H-NS regulated locus pairs (25 out of 26 pairs) yielded crosslinking frequency values larger than the background level, all of which showed reduced crosslinking frequency values upon *hns* deletion, suggesting protein-induced juxtaposition of these loci (Fig. 4B, left). Taken together, these results indicate that the H-NS clusters bring many gene loci into proximity and thereby mediate long-range interactions in the chromosome.

Overall, our results demonstrate that H-NS forms a few compact clusters in the chromosome, with cluster formation driven by oligomerization of H-NS bound to DNA. The genes regulated by H-NS are specifically sequestered into these clusters. Given that H-NS is a global transcriptional silencer that regulates ~5% of all *E. coli* genes (*43*) and binds to many DNA sites broadly distributed along the *E. coli* genome (*8-9, 11-13*), the cluster formation of H-NS and, consequently, the juxtaposition of DNA segments interacting with H-NS must cause substantial folding and condensation of the bacterial DNA. The H-NS clusters could thus serve as anchoring points for numerous DNA loci distributed throughout the genome, potentially creating DNA loops connecting the anchored loci. These anchor points (or organizing centers) can act in concert with the previously described chromosome domains (*4-5*) to shape the 3D architecture of the *E. coli* chromosome.

Supplementary Material

Refer to Web version on PubMed Central for supplementary material.

Acknowledgments

Reference

1. Robinow C, Kellenberger E. Microbiol Rev. 1994; 58:211. [PubMed: 7521510]

2. Eltsov M, Zuber B. J Struct Biol. 2006; 156:246. [PubMed: 16978880]

3. Gitai Z, Thanbichler M, Shapiro L. Trends Microbiol. 2005; 13:221. [PubMed: 15866039]

4. Reyes-Lamothe R, Wang X, Sherratt D. Trends Microbiol. 2008; 16:238. [PubMed: 18406139]

5. Espeli O, Boccard F. J Struct Biol. 2006; 156:304. [PubMed: 16979349]

6. Johnson, RC.; Johnson, LM.; Schmidt, JW.; Gardner, JF. Chapter 1.5. In: Higgins, NP., editor. The Bacterial Chromosome. ASM Press; Washington, D.C.: 2005.

7. Dillon SC, Dorman CJ. Nat Rev Microbiol. 2010; 8:185. [PubMed: 20140026]

8. Grainger DC, Hurd D, Goldberg MD, Busby SJ. Nucleic Acids Res. 2006; 34:4642. [PubMed: 16963779]

9. Oshima T, Ishikawa S, Kurokawa K, Aiba H, Ogasawara N. DNA Res. 2006; 13:141. [PubMed: 17046956]

10. Li G-W, Berg OG, Elf J. Nat Phys. 2009; 5:294.

11. Navarre WW, et al. Science. 2006; 313:236. [PubMed: 16763111]

12. Lucchini S, et al. PLoS Pathog. 2006; 2:e81. [PubMed: 16933988]

13. Lang B, et al. Nucleic Acids Res. 2007; 35:6330. [PubMed: 17881364]

14. Dorman CJ. Nat Rev Microbiol. 2004; 2:391. [PubMed: 15100692]

15. Fang FC, Rimsky S. Curr Opin Microbiol. 2008; 11:113. [PubMed: 18387844]

16. McGovern V, Higgins NP, Chiz RS, Jaworski A. Biochimie. 1994; 76:1019. [PubMed: 7748923]

17. Smyth CP, et al. Mol Microbiol. 2000; 36:962. [PubMed: 10844682]

18. Rimsky S. Curr Opin Microbiol. 2004; 7:109. [PubMed: 15063845]

19. Dame RT, Noom MC, Wuite GJ. Nature. 2006; 444:387. [PubMed: 17108966]

20. Liu Y, Chen H, Kenney LJ, Yan J. Genes Dev. 2010; 24:339. [PubMed: 20159954]

21. Vora T, Hottes AK, Tavazoie S. Mol Cell. 2009; 35:247. [PubMed: 19647521]

22. Deich J, Judd EM, McAdams HH, Moerner WE. Proc Natl Acad Sci U S A. 2004; 101:15921. [PubMed: 15522969]

23. Elf J, Li GW, Xie XS. Science. 2007; 316:1191. [PubMed: 17525339]

24. Taniguchi Y, et al. Science. 2010; 329:533. [PubMed: 20671182]

25. Rust MJ, Bates M, Zhuang X. Nat Methods. 2006; 3:793. [PubMed: 16896339]

26. Betzig E, et al. Science. 2006; 313:1642. [PubMed: 16902090]

27. Hess ST, Girirajan TP, Mason MD. Biophys J. 2006; 91:4258. [PubMed: 16980368]

28. Biteen JS, et al. Nat Methods. 2008; 5:947. [PubMed: 18794860]

29. Huang B, Babcock H, Zhuang X. Cell. 2010; 143:1047. [PubMed: 21168201]

30. McKinney SA, Murphy CS, Hazelwood KL, Davidson MW, Looger LL. Nat Methods. 2009; 6:131. [PubMed: 19169260]

31. Supporting material is available on *Science* online.

32. Huang B, Wang W, Bates M, Zhuang X. Science. 2008; 319:810. [PubMed: 18174397]

33. Egner A, et al. Biophys J. 2007; 93:3285. [PubMed: 17660318]

34. Lee SF, Thompson MA, Schwartz MA, Shapiro L, Moerner WE. Biophys J. 2011; 100:L31. [PubMed: 21463569]

35. Smits WK, Grossman AD. PLoS Genet. 2010; 6:e1001207. [PubMed: 21085634]

36. Ueguchi C, Seto C, Suzuki T, Mizuno T. J Mol Biol. 1997; 274:145. [PubMed: 9398522]

37. Spurio R, Falconi M, Brandi A, Pon CL, Gualerzi CO. EMBO J. 1997; 16:1795. [PubMed: 9130723]

38. Badaut C, et al. J Biol Chem. 2002; 277:41657. [PubMed: 12200432]

39. Subach FV, et al. Nat Methods. 2009; 6:153. [PubMed: 19169259]

40. Schumann, W. Dynamics of the bacterial chromosome. Wiley-VCH Weinheim; Germany: 2006. Chapter 2.2.

41. Reidl J, Boos W. J Bacteriol. 1991; 173:4862. [PubMed: 1856179]

42. Dekker J, Rippe K, Dekker M, Kleckner N. Science. 2002; 295:1306. [PubMed: 11847345]

43. Hommais F, et al. Mol Microbiol. 2001; 40:20. [PubMed: 11298273]

44. Datsenko KA, Wanner BL. Proc Natl Acad Sci U S A. 2000; 97:6640. [PubMed: 10829079]

45. Xiao, JEJ.; Li, G-W.; YU, J.; Xie, XS. Single Molecule Techniques: A Laboratory Manual. Selvin, P.; Ha, T., editors. Cold Spring Harbor Laboratory Press; 2007. p. 149-170.

46. Huang B, Jones SA, Brandenburg B, Zhuang X. Nat Methods. 2008; 5:1047. [PubMed: 19029906]

47. Bates M, Huang B, Dempsey GT, Zhuang X. Science. 2007; 317:1749. [PubMed: 17702910]

48. Chodavarapu S, Felczak MM, Yaniv JR, Kaguni JM. Mol Microbiol. 2008; 67:781. [PubMed: 18179598]

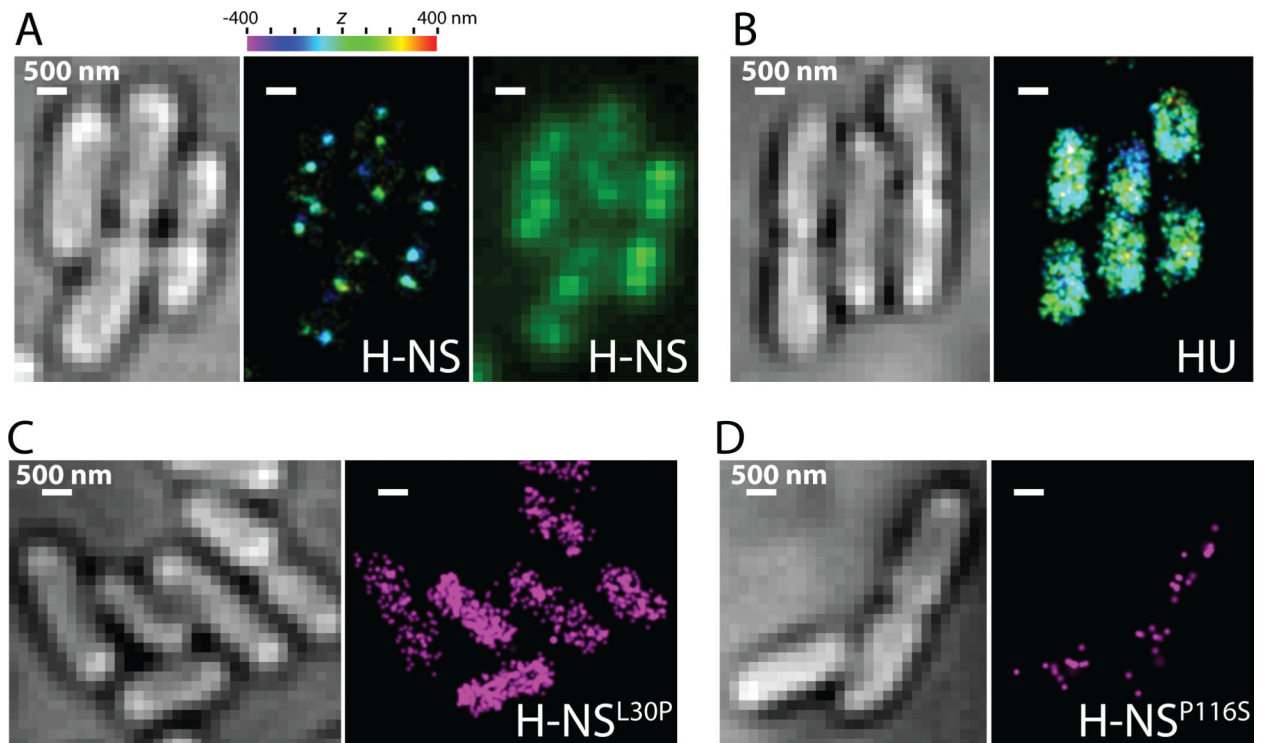49. Sonnenfield JM, Burns CM, Higgins CF, Hinton JC. Biochimie. 2001; 83:243. [PubMed: 11278075]

**Fig. 1.**
Super-resolution imaging of major nucleoid-associated proteins in living *E. coli* cells. (**A**) Compact H-NS clusters in the nucleoid. The *E. coli* cells shown in the bright-field image (left) expressed photoactivatable fluorescent protein mEos2 fused to H-NS, which was imaged with sub-diffraction-limit resolution (middle). The *z*-coordinate of each localization in the 3D STORM image is color-coded according to the color bar. In comparison, a conventional fluorescence image of the same cells is shown (right). A time-lapse movie corresponding to the super-resolution image is shown in Movie S1 (*31*). Due to the slow cluster movements, the images of H-NS are not motion-blurred appreciably. (**B**) Scattered distribution of HU in the nucleoid. Left, bright-field image. Right, 3D STORM image of mEos2-labeled HU in the same cells. Similar distributions were observed for Fis, IHF and StpA (Fig. S2) (*31*). Fine features of the nucleoid shape could potentially be blurred by movement. (**C**, **D**) Dependence of H-NS cluster formation on its oligomerization and DNA-binding capabilities. (**C**) Bright field image of cells (left) and corresponding 2D super-resolution image of H-NS (right) with a point mutation, L30P, that inhibits dimerization/ oligomerization. (**D**) Bright field image (left) and corresponding 2D super-resolution image of H-NS (right) with a point mutation, P116S, that inhibits DNA binding. Image acquisition time: 0.5 – 2 min for each image.
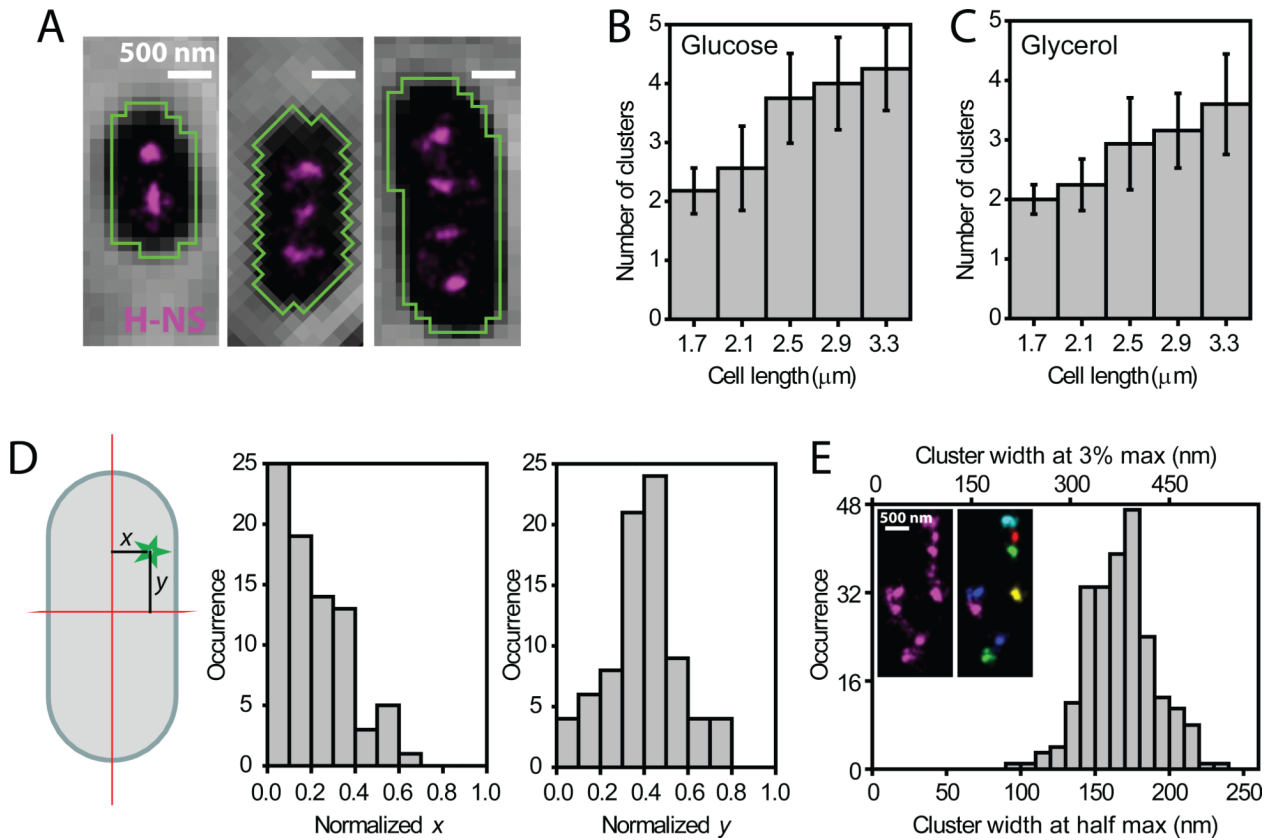
Fig. 2.
Quantitative characterizations of the H-NS clusters. (**A-C**) The number of clusters per cell.
(**A**) Overlay of the phase contrast images showing the cell contours (segmentation shown in
green) and the super-resolution images of H-NS (magenta) for three cells of different
lengths. (**B, C**) The average number of clusters per cell versus the cell length is shown for
different growth conditions (medium supplemented with glucose (B) or glycerol (C)). Error
bars: SD (N = 28, 32, 32, 14, and 4 cells from left to right for (B) and N = 34, 49, 31, 32, and
10 cells from left to right for (C)). (**D**) The location of clusters. Each cluster (green) was
assigned a coordinate (x, y) relative to the cell axes (left). For cells with two clusters, the
distributions of cluster coordinates are plotted for x normalized to the half cell width and y
normalized to the half cell length. For cells with three clusters, the (x, y) distributions are
shown in Fig S5 (*31*). (**E**) The size of clusters. The distribution of the full width at half
maximum (FWHM, bottom axis) or full width at 3% maximum (top axis) of the clusters was
determined with automated cluster identification (example image (left) and segmentation
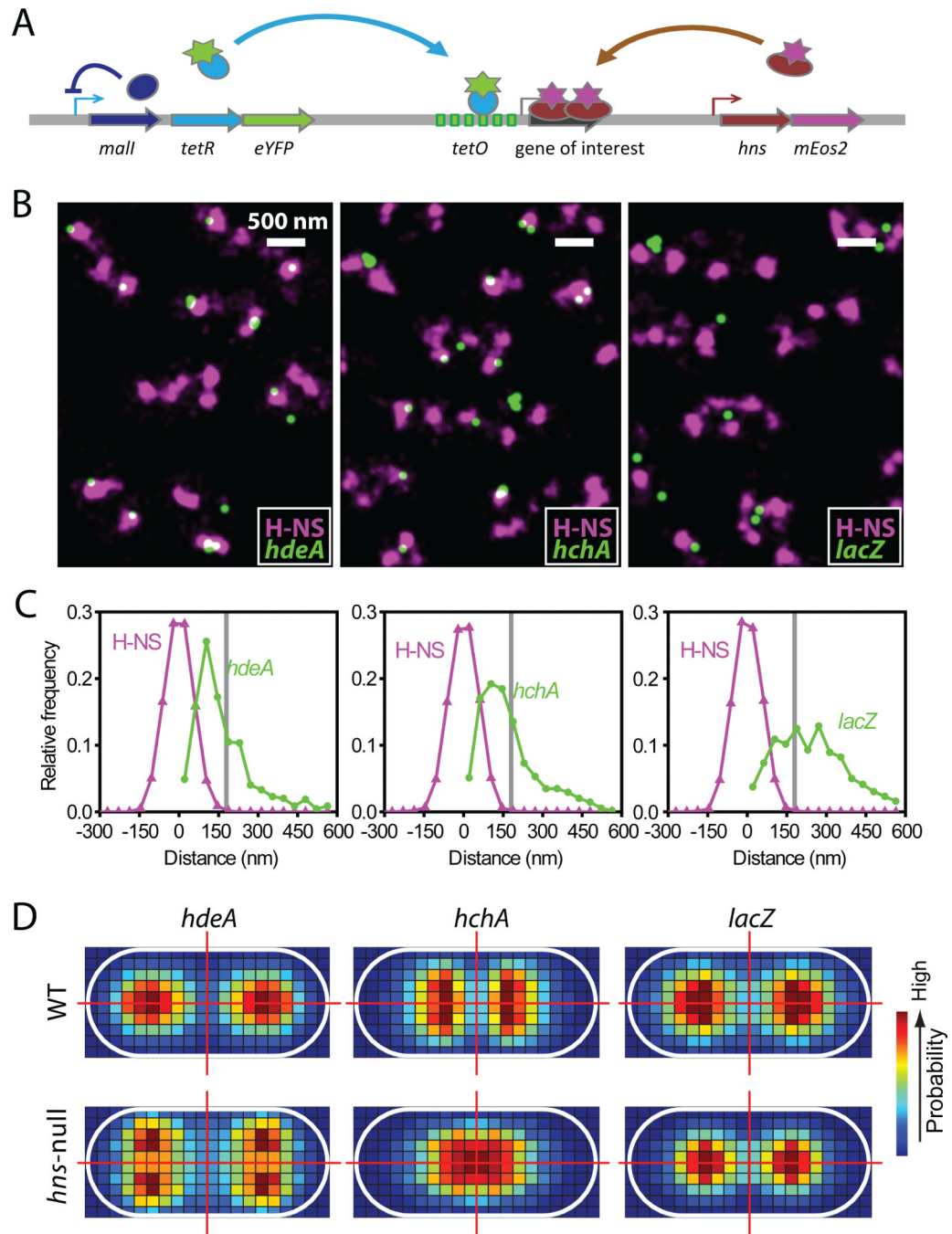(right) shown in inset) (*31*). Image acquisition time: 1 min.

Fig. 3.
Colocalization of H-NS clusters and specific gene loci. (**A**) Two-color imaging scheme of mEos2-labeled H-NS and eYFP-labeled gene locus as described in the text. (**B**) Two-color live-cell images of H-NS (magenta) and the *hdeA, hchA*, or *lacZ* loci (green), showing more extensive H-NS co-localization for *hdeA* and *hchA*. Because each blinking event of eYFP was imaged independently, a single gene locus may appear as more than one puncta. (**C**) Quantitative co-localization analysis between H-NS clusters and the *hdeA, hchA*, or *lacZ* loci. Green curves: the 2D-distance distributions between the gene loci and the center positions of their nearest H-NS clusters; magenta curves: the density cross-sections of these H-NS clusters aligned to their center positions. About 67% of *hdeA*, 65% of *hchA*, and 36%

lacZ loci resided within the boundary of the clusters (defined by the grey lines, positioned at 3% of the peak values of the magenta curves) (*31*). The 3% line was chosen as the cluster boundary because the background density outside the clusters was only ~1% of the peak densities. The colocalization fraction of *lacZ* is close to the expected background value (20-30%), derived from a random distribution of the gene locus in the nucleoid. To remove the potential artifact due to cluster size heterogeneity associated with this ensemble analysis, we performed an alternative single-locus-based analysis, which also showed that *hdeA* and *hchA* colocalized with H-NS clusters to a substantially higher degree than *lacZ* (*31*). In each case, 500-700 gene locus positions were analyzed. (**D**) Displacement of gene loci upon H-NS deletion. Plotted are the 2D histograms of the relative *hdeA, hchA*, and *lacZ* locus positions normalized to the cell dimensions. Considering the approximate mirror symmetry of the cell shape along its long and short axes observed in the bright-field images, we placed normalized locus positions into the first quartile of the cell and then extended the probability density map into the other three quartiles by enforcing the mirror symmetry. Therefore, symmetric peaks within the cell do not necessarily reflect the presence of more than one most probable positions of the gene locus. The grid size is ~100-200 nm and the probability density is color-coded according to the color bar (right). The cell outlines are shown as white ovals and the cell axes are shown as red lines. In each case, 2000-5000 gene locus positions were analyzed.
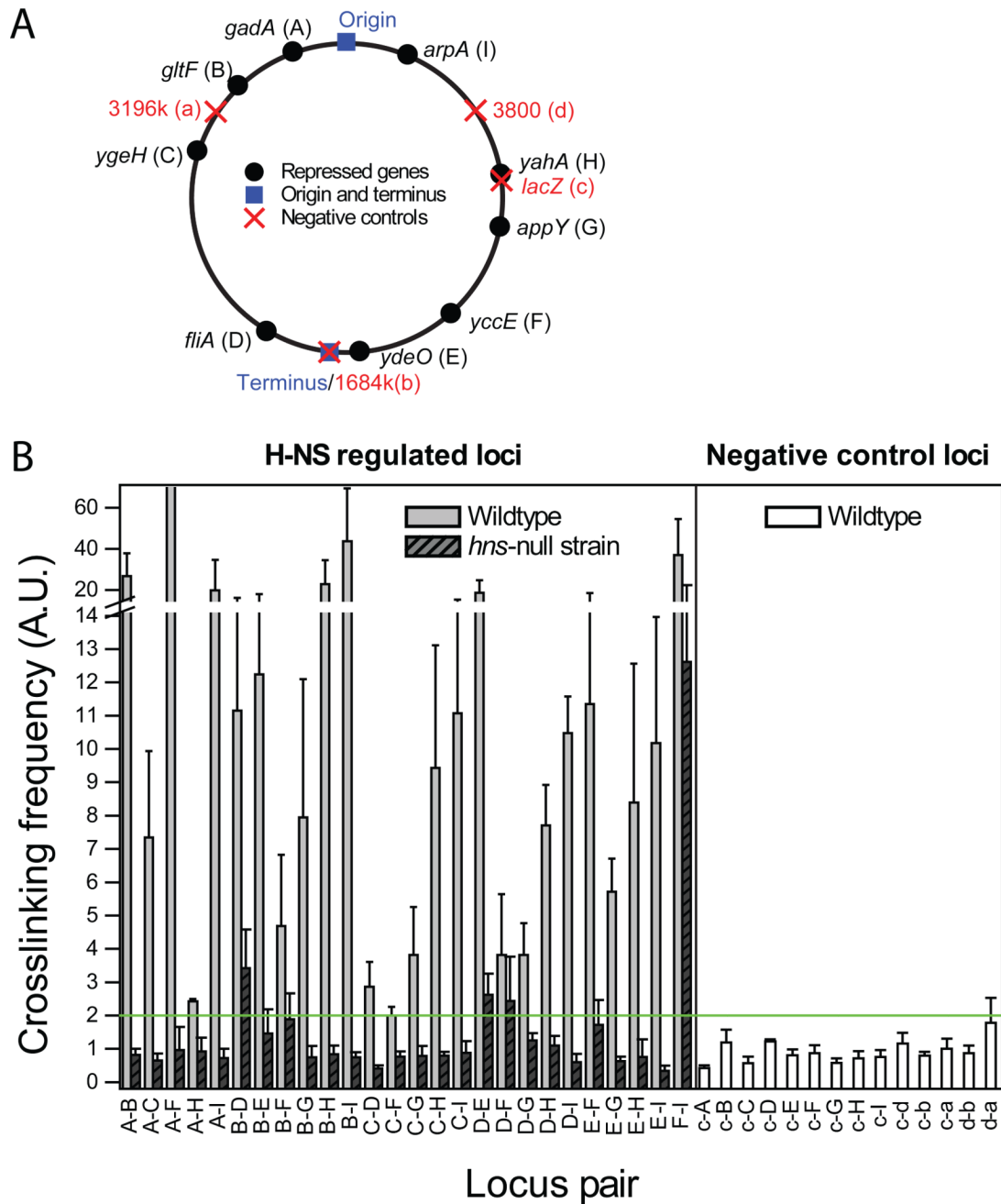
Fig. 4.
Proximity between gene locus pairs probed by chromosome conformation capture (3C). **(A)** Nine H-NS regulated gene loci (labeled as A-I, black circles) and four negative control loci (labeled as a-d, red crosses) on the circular *E. coli* chromosome map. The origin and terminus of replication are marked with blue squares as position references. **(B)** Crosslinking frequencies between pairs of chromosome loci. The crosslinking efficiency is defined as the ratio of qPCR signals between the crosslinked sample and the non-crosslinked control. Each column represents one pair of H-NS regulated loci (grey bars), or one pair involving at least one negative control loci (white bars). The crosslinking frequencies of the *hns*-null cells are shown for the regulated pairs in dark grey, hashed bars. The green line marks a 2-fold difference between crosslinked and non-crosslinked cells. These data reflect the population

average behavior and the proximity pattern between the gene locus pairs could vary from cell to cell. Error bars: SEM (N = 3 sets of independent experiments).